

Supplementary Material

Combining Microcosm Biodegradation and Reactive Transport Modeling to Explore the Feasibility of ATES-Bioremediation Approaches

**Henning Wienkenjohann¹, Mohammad Sufian Bin Hudari², Klaus Mosthaf¹, Carsten Vogt²,
Ivonne Nijenhuis², Massimo Rolle^{1,3*}**

¹Department of Environmental and Resource Engineering, Technical University of Denmark, Kgs. Lyngby, Denmark

²Department of Isotope Biogeochemistry, Helmholtz Centre for Environmental Research - UFZ, Leipzig, Germany

³Institute of Applied Geosciences, Department of Materials and Geosciences, Technical University of Darmstadt, Darmstadt, Germany

*Corresponding author phone: +49 (0) 61 51 16-23577

email: massimo.rolle@tu-darmstadt.de

1 Temperature-dependence of physical and chemical properties

The physical properties of the water fluid, i.e., water density, dynamic viscosity, specific isobaric heat capacity, and thermal conductivity, are dependent on temperature. We used the IF97 formulation (Wagner et al., 2000; IAPWS, 2007), as detailed by Wienkenjohann et al. (2024), to accurately describe non-isothermal fluid flow in the models.

The temperature dependence of the aqueous solubility of TCE is important for the accurate description of the mass transfer from the TCE NAPL phase to the aqueous TCE phase. The temperature dependence was implemented using the empirical model and experimental data reported in Koproch et al. (2019). We used a subset of that dataset, considering the temperature range from 5 to 40 °C (Fig. S1a).

To account for the effect of temperature on the aqueous diffusion coefficient of chlorinated ethenes we implemented the equation by Worch (1993) (Eq. 17 in manuscript). Fig. S1b shows that the aqueous diffusion coefficients increase with increasing temperatures.

For the batch multi-phase biodegradation modeling, we also considered the temperature dependence of Henry's law constant to accurately describe the mass transfer between the aqueous and the gaseous phase. Partition coefficients for common chlorinated ethenes are known at room temperature T_{ref} (Gossett, 1987; Sander, 2023). The van't Hoff equation can be used to extrapolate to other temperatures T_2 :

$$H_{T_2,i} = H_{T_{ref},i} \exp\left(B_i \left(\frac{1}{T_{ref}} - \frac{1}{T_2}\right)\right) \quad S1$$

here $H_{T_2,i}$ and $H_{T_{ref},i}$ are Henry's law constants at the temperatures T_2 and T_{ref} in Kelvin for the i -th species, and $B_i = \Delta H_{Henry,i}/R$ is a temperature correction factor with the enthalpy $\Delta H_{Henry,i}$ and the gas constant R . Values of $H_{T_{ref},i}$ and B_i are reported in Gossett (1987) and Sander (2023) for various organic compounds. Fig. S1c shows the temperature dependence of the chlorinated ethenes considered in this study. The Henry's law constants of vinyl chloride and particularly ethene show a strong temperature effect.

In both the batch microcosms and the field-scale scenario simulations, we implemented the dependence of the soil organic carbon – water partition coefficient K_{OC} on temperature using the van't Hoff equation:

$$K_{OC,T_2,i} = K_{OC,T_{ref},i} \exp\left(\frac{\Delta H_{sorption,i}}{R} \left(\frac{1}{T_{ref}} - \frac{1}{T_2}\right)\right) \quad S2$$

with $K_{OC,T_2,i}$ and $K_{OC,T_{ref},i}$ the soil organic carbon – water partition coefficients at the temperatures T_2 and T_{ref} in Kelvin for the i -th species, and $\Delta H_{sorption,i}$ the species-specific sorption enthalpy. Data on the sorption enthalpy for chlorinated ethenes is scarce. We used the sorption enthalpy for TCE as -2

kJ/mol (Heron et al., 1998). Fig. S1d shows the strongest temperature effect for TCE and less pronounced effects for the other compounds.

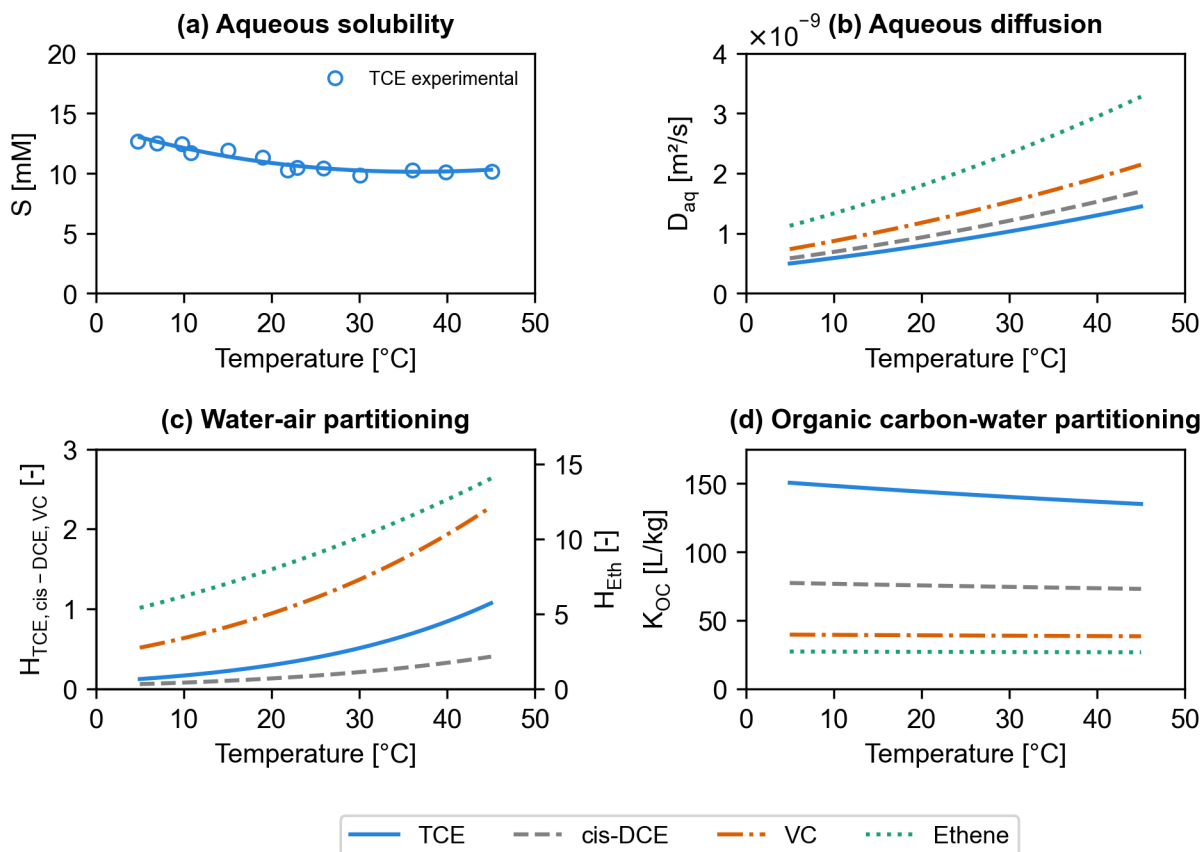


Figure S1 Temperature dependence of the aqueous solubility of TCE (experimental data (circles) taken from Koproch et al. (2019)) (a); the aqueous diffusion coefficients D_{aq} (b); the Henry's law constants H (c); and the K_{OC} values (d) for TCE, cis-DCE, VC, and ethene.

2 Physical and chemical heterogeneity in the field-scale scenario models

2.1 Contaminant source zone

The source zone of the parent compound TCE was placed in the center of the model domain in between the injection and the abstraction wells. In all scenario simulations, TCE was implemented as NAPL phase and dissolved in the aqueous phase. The TCE concentration fields were created by running another stand-alone simulation (initial concentration: 0.3 mM) considering only diffusive mass transport. This resulted in smooth concentration gradients at the outer boundaries of the TCE source zone at the last time step of the simulation (Fig. S2). The result was exported as grid file and used as initial condition at $t = 0$ days for TCE solute transport in all model scenarios listed in Tab. 1.

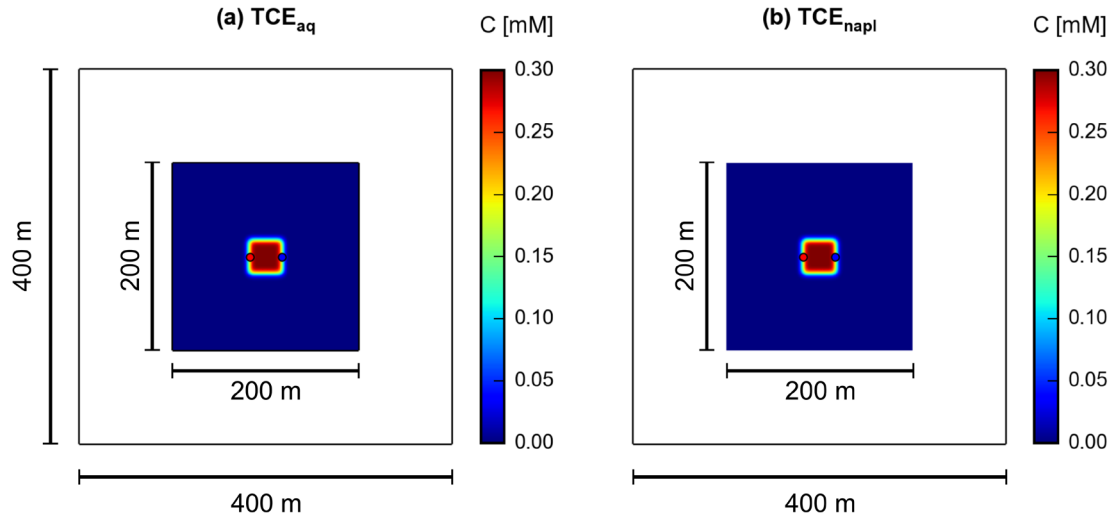


Figure S2 Surface maps of initial concentrations at $t = 0$ days of TCE in the aqueous phase (a) and in the NAPL phase (b) as used in all scenario simulations. Large solution domain ($400 \text{ m} \times 400 \text{ m}$) for fluid flow and heat transport and small solution domain ($200 \text{ m} \times 200 \text{ m}$) for solute transport. Injection and abstraction wells are indicated by the red and blue dots, respectively.

2.2 Spatially-varying properties of the subsurface porous media

We used the hydraulic conductivity statistics of the well-characterized Borden aquifer (Sudicky, 1986). Tab. S1 shows the parameters used in this study.

Table S1 Properties of the heterogeneous hydraulic conductivity field.

| Parameter | Value |
|---|-----------------------|
| Geometric mean of K [m s^{-1}] | 7.17×10^{-5} |
| Variance σ^2 of $\ln(K)$ | 0.29 |
| Integral scales I_x and I_y [m] | 2.8; 2.8 |

Fig. S3 shows the probability distribution for important physico-chemical parameters of the heterogeneous aquifer system considered in the field-scale scenario simulations. These probability density functions were used in all model scenarios.

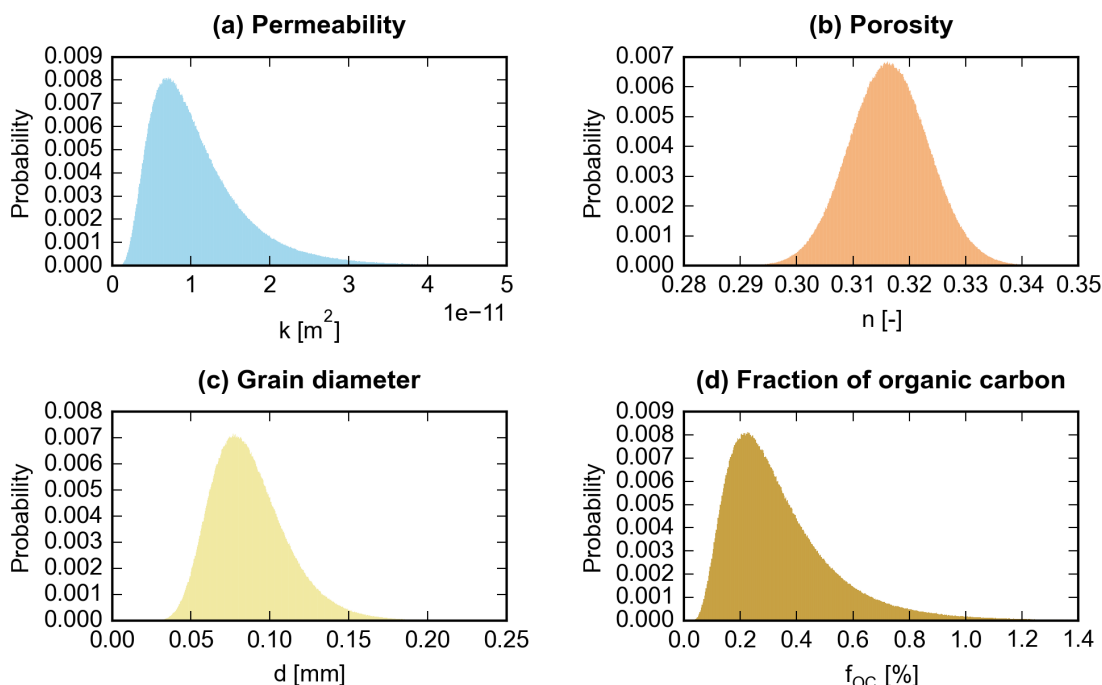


Figure S3 Probability density functions of porous media characteristics: permeability (a), porosity (b), grain diameter (c), and fraction of organic carbon (d) in the field scale domain.

3 Additional results from the scenario simulations

We report additional results on the effect of the natural groundwater flow velocity on the bioremediation efficiency. The scenarios S5a, S5b, and S5c lead to very low biodegradation (results not shown). The combination of low pumping rate, low injection temperature, and low lactate concentration creates unsuitable conditions for the specialized degraders to transform TCE to ethene. Only minor amounts of cis-DCE are formed. In addition, the natural groundwater flow velocity has no major influence on the overall biodegradation potential in the scenarios S5a, S5b, and S5c.

On the contrary, the natural groundwater flow velocity influences the amount of degraded contaminant masses when considering intermediate operational procedures as illustrated in Fig. S4. Fig. S4 shows scenarios with intermediate operational parameters, i.e., higher absolute values than the ones considered in the previous scenarios (scenarios S5a, S5b, and S5c), but lower than the optimal parameters used in the scenarios shown in Fig. 8 in the main manuscript (scenarios S0, S1a, and S1b). The combination of higher overall pumping rate, increased injection temperature, and higher lactate concentration stimulates biotransformation. However, the transformation from the parent compound (TCE) to the non-toxic end product (ethene) is not complete. Vinyl chloride is accumulating at 100 to 200 days (Fig. S4c). The scenarios at intermediate operational procedures are performing worse compared to the scenarios considering high/optimal operational procedures, in which complete biotransformation occurred (Fig. 8, main manuscript). The effect of the natural groundwater flow velocity on the bioremediation efficiency is different when considering intermediate and optimal operational procedures. Fig. S4 shows that ATES-ISB systems under low flow conditions, i.e., 8 m/year, result in faster biotransformation, while fast flow conditions (i.e., 80 m/year) result in slower

biotransformation of the chlorinated ethenes. Interestingly, the overall biotransformation is more complete and faster at the highest natural groundwater flow velocity (i.e., 80 m/year), when considering optimal operational procedures (Fig. 8). This might be caused by solute mixing effects at different natural groundwater flow velocities.

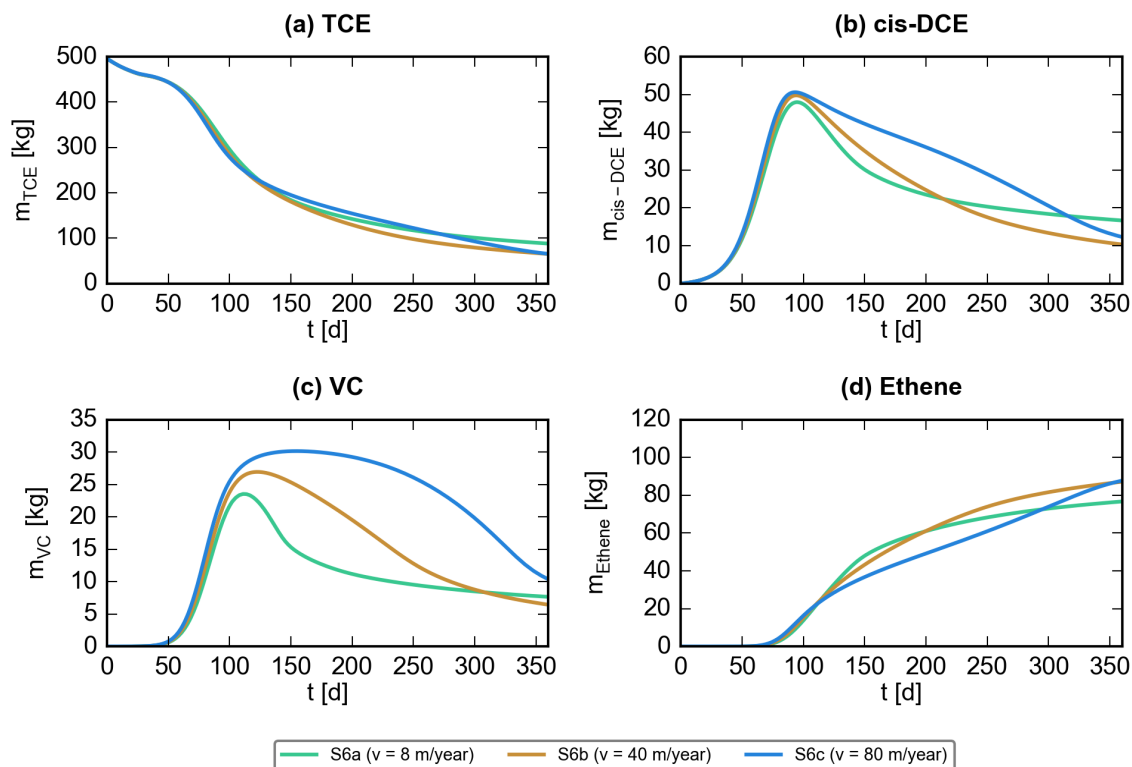


Figure S4 Comparison of total masses of chlorinated ethenes for the scenarios S6a, S6b, and S6c. Additional results of scenario simulations considering the natural groundwater flow velocity as parameter of interest. Scenarios with intermediate pumping rate ($10 \text{ m}^3/\text{hour}$), intermediate injection temperature ($20 \text{ }^\circ\text{C}$), and intermediate injected lactate concentration (0.02 mM).

4 Data and input for the model

Table S2 Input parameters for the batch multi-phase modeling of the microcosms.

| Parameter | Description | Unit | Value |
|-------------------|---|--------------------|----------------------------|
| T | Temperature of the microcosms | °C | 10; 20; 30; 40 |
| V_{tot} | Total volume of the Wheaton serum bottle | ml | 125 ^a |
| V_{aq} | Volume of the aqueous phase | ml | 50 ^a |
| m_s | Mass of the sediment | g | 20 ^a |
| ρ_b | Bulk density of the sediment | g cm ⁻³ | 1.2 ^b |
| f_{OC} | Fraction of organic carbon of the sediment | % | 0.5 ^b |
| A_{aq-sed} | Area of the water-sediment interface | cm ² | 24 |
| A_{aq-gas} | Area of the water-gas interface | cm ² | 43 |
| κ_{aq-sed} | Mass-transfer coefficients at interface water-sediment | cm h ⁻¹ | 0.35 ^c |
| κ_{aq-gas} | Mass-transfer coefficients at interface water-gas | cm h ⁻¹ | 0.47 ^c |
| H_{TCE} | Henry's law constant of TCE | - | Fig. S1c |
| H_{DCE} | Henry's law constant of DCE | - | Fig. S1c |
| H_{VC} | Henry's law constant of VC | - | Fig. S1c |
| H_{Eth} | Henry's law constant of ethene | - | Fig. S1c |
| $K_{OC,TCE}$ | Soil organic carbon – water partition coefficient of TCE | L kg ⁻¹ | Fig. S1d |
| $K_{OC,DCE}$ | Soil organic carbon – water partition coefficient of DCE | L kg ⁻¹ | Fig. S1d |
| $K_{OC,VC}$ | Soil organic carbon – water partition coefficient of VC | L kg ⁻¹ | Fig. S1d |
| $K_{OC,Eth}$ | Soil organic carbon – water partition coefficient of ethene | L kg ⁻¹ | Fig. S1d |
| $c_{0,Lac}$ | Lactate concentration at day 0 | mM | 3 ^a |
| $c_{spike,TCE}$ | Concentration of TCE spikes | μM | 100 ^a |
| $t_{spike,TCE}$ | Time of TCE spikes | d | 3; 35; 56; 70 ^a |

^a Bin Hudari et al. (2025); ^b Filippini et al. (2016); ^c Model assumption

Table S3 Results of the biodegradation modeling of the microcosms.

| Parameter | Description | Unit | Value |
|---------------------------------|--|-----------------|-----------------------|
| $\kappa_{max,TCE}(10^{\circ}C)$ | Max. specific degradation rate of TCE with <i>Dhc</i> at 10 °C | s ⁻¹ | 3.14×10^{-5} |
| $\kappa_{max,DCE}(10^{\circ}C)$ | Max. specific degradation rate of DCE with <i>Dhc</i> at 10 °C | s ⁻¹ | 2.60×10^{-5} |
| $\kappa_{max,VC}(10^{\circ}C)$ | Max. specific degradation rate of VC with <i>Dhc</i> at 10 °C | s ⁻¹ | 1.99×10^{-5} |
| $\kappa_{max,TCE}(20^{\circ}C)$ | Max. specific degradation rate of TCE with <i>Dhc</i> at 20 °C | s ⁻¹ | 7.75×10^{-5} |
| $\kappa_{max,DCE}(20^{\circ}C)$ | Max. specific degradation rate of DCE with <i>Dhc</i> at 20 °C | s ⁻¹ | 5.51×10^{-5} |
| $\kappa_{max,VC}(20^{\circ}C)$ | Max. specific degradation rate of VC with <i>Dhc</i> at 20 °C | s ⁻¹ | 3.86×10^{-5} |
| $\kappa_{max,TCE}(30^{\circ}C)$ | Max. specific degradation rate of TCE with <i>Dhc</i> at 30 °C | s ⁻¹ | 1.08×10^{-4} |
| $\kappa_{max,DCE}(30^{\circ}C)$ | Max. specific degradation rate of DCE with <i>Dhc</i> at 30 °C | s ⁻¹ | 6.61×10^{-5} |
| $\kappa_{max,VC}(30^{\circ}C)$ | Max. specific degradation rate of VC with <i>Dhc</i> at 30 °C | s ⁻¹ | 4.25×10^{-5} |
| $\kappa_{max,TCE}(40^{\circ}C)$ | Max. specific degradation rate of TCE with <i>Dhc</i> at 40 °C | s ⁻¹ | 7.38×10^{-6} |
| $\kappa_{max,DCE}(40^{\circ}C)$ | Max. specific degradation rate of DCE with <i>Dhc</i> at 40 °C | s ⁻¹ | 1.07×10^{-5} |
| $\kappa_{max,VC}(40^{\circ}C)$ | Max. specific degradation rate of VC with <i>Dhc</i> at 40 °C | s ⁻¹ | 4.68×10^{-6} |

Table S4 Aquifer and geometry parameters for the field-scale scenario simulations.

| Parameter | Description | Unit | Value |
|------------------|--|----------------|------------------|
| k | Permeability | m ² | Fig. S3a |
| n | Porosity | – | Fig. S3b |
| d | Grain diameter | mm | Fig. S3c |
| b | Modeled aquifer thickness | m | 6 ^b |
| $l_{nj,abst}$ | Length between injection and abstraction well | m | 30 ^b |
| $d_{inj,abst}$ | Borehole diameter, injection, and abstraction well | mm | 254 ^b |

^a Derived from permeability field; ^b Model assumption

Table S5 Thermal input parameters for the field-scale scenario simulations.

| Parameter | Description | Unit | Value |
|------------------|---------------------------------|-----------------------------------|------------------------|
| $T_{initial}$ | Initial groundwater temperature | °C | 10 ^a |
| γ_L | Longitudinal heat dispersivity | m | 0.1 ^b |
| γ_T | Transverse heat dispersivity | m | 0.01 ^b |
| $c_{p,s}$ | Specific heat capacity, solid | J kg ⁻¹ K | 730.566 ^{b,c} |
| λ_s | Thermal conductivity, solid | W m ⁻¹ K ⁻¹ | 3.0 ^{b,c} |

^a Model assumption; ^b Beyer et al. (2016); ^c Calculated based on VDI (2010)

Table S6 Input parameters for solute transport in the field-scale scenario simulations.

| Parameter | Description | Unit | Value |
|---------------------|--|--------------------------------|----------------------|
| M_{TCE} | Molecular weight, TCE | g mol ⁻¹ | 131.388 ^b |
| M_{DCE} | Molecular weight, cis-DCE | g mol ⁻¹ | 96.943 ^b |
| M_{VC} | Molecular weight, VC | g mol ⁻¹ | 62.498 ^b |
| M_{Eth} | Molecular weight, ethene | g mol ⁻¹ | 28.053 ^b |
| M_{Lac} | Molecular weight, lactate | g mol ⁻¹ | 90.0795 ^b |
| M_{DOC} | Atomic weight, DOC (considered as carbon) | g mol ⁻¹ | 12 ^c |
| $c_{init,TCE}$ | Initial concentration, TCE _{aqueous} | mM | 0.3 (Fig. S2) |
| $c_{init,TCE,NAPL}$ | Initial concentration, TCE _{NAPL} | mM | 0.3 (Fig. S2) |
| $c_{init,DCE}$ | Initial concentration, cis-DCE | mM | 0 ^d |
| $c_{init,VC}$ | Initial concentration, VC | mM | 0 ^d |
| $c_{init,Eth}$ | Initial concentration, ethene | mM | 0 ^d |
| $c_{init,Lac}$ | Initial concentration, lactate | mM | 0 ^d |
| $c_{init,DOC}$ | Initial concentration, DOC | mM | 0.125 ^d |
| ω_i | Mass transfer rate, TCE _{aqueous} – TCE _{NAPL} | d ⁻¹ | 0.001 ^e |
| S_{TCE} | Aqueous solubility, TCE | mM | Fig. S1a |
| D_{TCE}^{aq} | Aqueous diffusion coefficient, TCE | m ² s ⁻¹ | Fig. S1b |
| D_{DCE}^{aq} | Aqueous diffusion coefficient, cis-DCE | m ² s ⁻¹ | Fig. S1b |
| D_{VC}^{aq} | Aqueous diffusion coefficient, VC | m ² s ⁻¹ | Fig. S1b |
| D_{Eth}^{aq} | Aqueous diffusion coefficient, ethene | m ² s ⁻¹ | Fig. S1b |
| f_{OC} | Fraction of organic carbon | % | Fig. S3d |
| $K_{OC,TCE}$ | Soil organic carbon – water partition coefficient of TCE | L kg ⁻¹ | Fig. S1d |
| $K_{OC,DCE}$ | Soil organic carbon – water partition coefficient of DCE | L kg ⁻¹ | Fig. S1d |
| $K_{OC,VC}$ | Soil organic carbon – water partition coefficient of VC | L kg ⁻¹ | Fig. S1d |
| $K_{OC,Eth}$ | Soil organic carbon – water partition coefficient of ethene | L kg ⁻¹ | Fig. S1d |

^a Simplified assumption based on Boving and Grathwohl (2001); ^b Lide et al. (2003); ^c Chapelle (2022); ^d Model assumption; ^e Illy et al. (2022)

Table S7 Biogeochemical input parameters for microcosms and field-scale scenario simulations.

| Parameter | Description | Unit | Value |
|--------------------|--|--|--------------------------------------|
| $T_{min,TCE}$ | Minimum growth temperature <i>Dhc</i> , TCE | °C | 3 ^a |
| $T_{min,DCE}$ | Minimum growth temperature <i>Dhc</i> , cis-DCE | °C | 1 ^a |
| $T_{min,VC}$ | Minimum growth temperature <i>Dhc</i> , VC | °C | 1 ^a |
| T_{max} | Maximum growth temperature | °C | 41 ^a |
| $T_{opt,TCE}$ | Optimum growth temperature <i>Dhc</i> , TCE | °C | 27.5 ^a |
| $T_{opt,DCE}$ | Optimum growth temperature <i>Dhc</i> , cis-DCE | °C | 26.0 ^a |
| $T_{opt,VC}$ | Optimum growth temperature <i>Dhc</i> , VC | °C | 25.0 ^a |
| $\mu_{opt,TCE}$ | Optimum growth constant <i>Dhc</i> , TCE | h ⁻¹ | 0.0277 ^a |
| $\mu_{opt,DCE}$ | Optimum growth constant <i>Dhc</i> , cis-DCE | h ⁻¹ | 0.017 ^a |
| $\mu_{opt,VC}$ | Optimum growth constant <i>Dhc</i> , VC | h ⁻¹ | 0.0111 ^a |
| $\kappa_{max,TCE}$ | Max. specific degradation rate, TCE | s ⁻¹ | Fig. 3a |
| $\kappa_{max,DCE}$ | Max. specific degradation rate, cis-DCE | s ⁻¹ | Fig. 3b |
| $\kappa_{max,VC}$ | Max. specific degradation rate, VC | s ⁻¹ | Fig. 3c |
| $X_{Dhc,0}$ | Initial biomass of <i>Dhc</i> bacteria in the field-scale domain | cells ml ⁻¹ | 5.3×10^4 ^b |
| Y | Microbial yield coefficient | mol _X mol _{EA} ⁻¹ | 0.02 ^c |
| b_{Dhc} | Biomass decay rate coefficient, <i>Dhc</i> bacteria | s ⁻¹ | 5.78×10^{-7} ^d |
| $K_{S,EDDOC}$ | Half-saturation constant of DOC | M | 9.59×10^{-5} ^b |
| $K_{S,EDLac}$ | Half-saturation constant of lactate | M | 9.59×10^{-5} ^c |
| $K_{S,EA_{TCE}}$ | Half-saturation constant of TCE | M | 1.00×10^{-5} ^e |
| $K_{S,EA_{DCE}}$ | Half-saturation constant of cis-DCE | M | 3.30×10^{-6} ^{f,g} |
| $K_{S,EA_{VC}}$ | Half-saturation constant of VC | M | 2.20×10^{-6} ^{f,g} |
| $K_{i,EA_{TCE}}$ | Inhibition constant of TCE | M | 1.00×10^{-5} ^d |
| $K_{i,EA_{DCE}}$ | Inhibition constant of cis-DCE | M | 3.60×10^{-6} ^d |
| $K_{i,EA_{VC}}$ | Inhibition constant of VC | M | 7.80×10^{-6} ^d |

^a Fitted with model from (Rosso et al., 1995) and output data from batch-scale modeling of microcosms (Tab. S3); ^b Model assumption; ^c Malaguerra et al. (2011); ^d Cupples et al. (2004); ^e Christ and Abriola (2007); ^f Friis et al. (2007); ^g Haston and McCarty (1999)

References

- Beyer, C., Popp, S., and Bauer, S. (2016). Simulation of temperature effects on groundwater flow, contaminant dissolution, transport and biodegradation due to shallow geothermal use. *Environ Earth Sci* 75, 1244. doi: 10.1007/s12665-016-5976-8
- Bin Hudari, M. S., Deb, S., Vogt, C., Filippini, M., and Nijenhuis, I. (2025). Temperature-associated effects on methanogenesis and microbial reductive dechlorination of trichloroethene in contaminated aquifer sediments. *Frontiers in Water* in preparation for this Special Issue.
- Boving, T. B., and Grathwohl, P. (2001). Tracer diffusion coefficients in sedimentary rocks: Correlation to porosity and hydraulic conductivity. *Journal of Contaminant Hydrology* 53, 85–100. doi: 10.1016/S0169-7722(01)00138-3
- Chapelle, F. H. (2022). *Dissolved Organic Carbon in Groundwater Systems*. The Groundwater Project.
- Christ, J. A., and Abriola, L. M. (2007). Modeling metabolic reductive dechlorination in dense non-aqueous phase liquid source-zones. *Advances in Water Resources* 30, 1547–1561. doi: 10.1016/j.advwatres.2006.05.024
- Cupples, A. M., Spormann, A. M., and McCarty, P. L. (2004). Comparative Evaluation of Chloroethene Dechlorination to Ethene by Dehalococcoides-like Microorganisms. *Environ. Sci. Technol.* 38, 4768–4774. doi: 10.1021/es049965z
- Filippini, M., Amorosi, A., Campo, B., Herrero-Martin, S., Nijenhuis, I., Parker, B. L., et al. (2016). Origin of VC-only plumes from naturally enhanced dechlorination in a peat-rich hydrogeologic setting. *Journal of Contaminant Hydrology* 192, 129–139. doi: 10.1016/j.jconhyd.2016.07.003
- Friis, A. K., Heimann, A. C., Jakobsen, R., Albrechtsen, H. J., Cox, E., and Bjerg, P. L. (2007). Temperature dependence of anaerobic TCE-dechlorination in a highly enriched Dehalococcoides-containing culture. *Water Research* 41, 355–364. doi: 10.1016/j.watres.2006.09.026
- Gossett, J. M. (1987). Measurement of Henry's Law Constants for C1 and C2 Chlorinated Hydrocarbons. *Environmental Science and Technology* 21, 202–208. doi: 10.1021/es00156a012
- Haston, Z. C., and McCarty, P. L. (1999). Chlorinated Ethene Half-Velocity Coefficients (K_S) for Reductive Dehalogenation. *Environ. Sci. Technol.* 33, 223–226. doi: 10.1021/es9805876
- Heron, G., Van Zutphen, M., Christensen, T. H., and Enfield, C. G. (1998). Soil Heating for Enhanced Remediation of Chlorinated Solvents: A Laboratory Study on Resistive Heating and Vapor Extraction in a Silty, Low-Permeable Soil Contaminated with Trichloroethylene. *Environ. Sci. Technol.* 32, 1474–1481. doi: 10.1021/es970563j
- IAPWS (2007). Revised Release R7-97 on the IAPWS Industrial Formulation 1997 for the Thermodynamic Properties of Water and Steam. *International Association for the Properties of Water and Steam*.

- Illy, V. D., Cohen, G. J. V., Verardo, E., Höhener, P., Guiserix, N., and Atteia, O. (2022). Using 1,1,1-Trichloroethane degradation data to understand NAPL dissolution and solute transport at real sites. *Journal of Contaminant Hydrology* 245, 103934. doi: 10.1016/j.jconhyd.2021.103934
- Koproch, N., Dahmke, A., and Köber, R. (2019). The aqueous solubility of common organic groundwater contaminants as a function of temperature between 5 and 70 °C. *Chemosphere* 217, 166–175. doi: 10.1016/j.chemosphere.2018.10.153
- Lide, D. R., Baysinger, G., Berger, L. I., Goldberg, R. N., Kehiaian, H. V., Kuchitsu, K., et al. (2003). *CRC Handbook of Chemistry and Physics Editor-in-Chief*.
- Malaguerra, F., Chambon, J. C., Bjerg, P. L., Scheutz, C., and Binning, P. J. (2011). Development and sensitivity analysis of a fully kinetic model of sequential reductive dechlorination in groundwater. *Environmental Science and Technology* 45, 8395–8402. doi: 10.1021/es201270z
- Rosso, L., Lobry, J. R., Bajard, S., and Flandrois, J. P. (1995). Convenient Model To Describe the Combined Effects of Temperature and pH on Microbial Growth. *Applied and Environmental Microbiology* 61, 610–616. doi: 10.1128/aem.61.2.610-616.1995
- Sander, R. (2023). Compilation of Henry's law constants (version 5.0.0) for water as solvent. *Atmos. Chem. Phys.* 23, 10901–12440. doi: 10.5194/acp-23-10901-2023
- Sudicky, E. A. (1986). A natural gradient experiment on solute transport in a sand aquifer: Spatial variability of hydraulic conductivity and its role in the dispersion process. *Water Resources Research* 22, 2047–2058.
- VDI (2010). Thermal use of the underground - Fundamentals, approvals, environmental aspects (VDI 4640 Blatt 1). Available at: <https://www.vdi.de/en/home/vdi-standards/details/vdi-4640-blatt-1-thermal-use-of-the-underground-fundamentals-approvals-environmental-aspects> (Accessed October 26, 2023).
- Wagner, W., Cooper, J. R., Dittmann, A., Kijima, J., Kretschmar, H.-J., Kruse, A., et al. (2000). The IAPWS Industrial Formulation 1997 for the Thermodynamic Properties of Water and Steam. *Journal of Engineering for Gas Turbines and Power* 122, 150–184. doi: 10.1115/1.483186
- Wienkenjohann, H., Mosthaf, K., Fischer, L. M., Bennedsen, L., Flyvbjerg, J., Christophersen, M., et al. (2024). Low-temperature Aquifer Thermal Energy Storage combined with in situ bioremediation of chlorinated ethenes: Pilot-scale observations and model-based interpretation. *Journal of Contaminant Hydrology* 267, 104421. doi: 10.1016/j.jconhyd.2024.104421
- Worch, E. (1993). Eine neue Gleichung zur Berechnung von Diffusionskoeffizienten gelöster Stoffe. *Vom Wasser* 81, 289–297.